Advances in Military Technology
Vol. 21, No. 1, 2026, pp. 163-175
ISSN 1802-2308, eISSN 2533-4123
DOI 10.3849/aimt.02029

Intra-Pulse Modulation Radar Signal Recognition Using I/Q Channels and Deep Learning

V. M. Duong*, T. P. Nguyen, V. D. Nguyen, V. T. Nguyen, and D. C. Nguyen

Faculty of Radio-Electronic Engineering, Le Quy Don Technical University Hanoi, Vietnam

The manuscript was received on 23 August 2025 and was accepted after revision for publication as an original research paper on 2 April 2026.

Abstract:

This paper proposes a new method for classifying and recognizing intra-pulse modulation radar signals based on the I/Q channel and convolutional neural networks. The method is structured into two main stages. In the first stage, features of the received signal, such as linear frequency modulation, Costas and polyphase codes, are determined using the I/Q channel. A deep learning network is designed for signal recognition in the second stage. The proposed method is evaluated using simulated signals in a MATLAB environment. The results show that, compared to the existing methods, it reduces training time and provides a higher average accuracy compared with classic method, making it suitable for hardware implementation.

Keywords:

intra-pulse modulation, recognition, deep learning, I/Q channels, Convolutional Neural Network (CNN), MATLAB simulation

1 Introduction

In the context of modern warfare, passive surveillance systems (PSS) have become increasingly significant due to their ability to operate without emitting signals, thus enhancing operational stealth compared to traditional active radars [1]. The primary function of PSS is to detect and classify electromagnetic sources, supporting the creation of an electronic order of battle. This is achieved by intercepting signals and estimating critical parameters such as carrier frequency, pulse width, pulse repetition interval, and modulation type [2].

Earlier generations of PSS lacked automated intra-pulse modulation analysis and relied heavily on operator expertise, which posed practical deployment challenges

* *Corresponding author: Van Minh Duong, Faculty of Radio-Electronic Engineering, Le Quy Don Technical University, Hanoi, Vietnam. E-mail: minhdv_k31@lqdtu.edu.vn. ORCID 0000-0002-8452-5044.*

[3, 4]. While current methodologies employed in PSS include the fast Fourier transform (FFT) [5], autocorrelation receivers [6], and frequency discriminators [7], recent advancements have focused on artificial intelligence (AI). Several AI-based techniques have emerged to recognize intra-pulse modulated radar signals with higher accuracy. For instance, Zhiyu Qu proposed a hybrid method combining convolutional neural networks (CNN) with deep Q-learning, utilizing Cohen's class time-frequency distributions (CTFD) to extract time-frequency images, achieving recognition accuracy exceeding 94 % even at low signal-to-noise ratios ($SNR = -6$ dB) [8]. Jingjing Cai developed a contrastive learning approach combined with the Choi-Williams distribution (CWD), achieving a recognition accuracy of 90 % at low $SNR = -8$ dB [9]. Another notable approach integrated CTFD with DGDNet (Deep Gradient Descent Network) to recognize 12 different modulated radar signals, demonstrating an accuracy of 98.2 % at Signal-to-Noise Ratio $SNR = -8$ dB [10]. The most recent technique involves supervised contrastive learning, which achieves comparable accuracy to other methods while requiring only 50 % of the number of samples [11].

Generally, these methods employ time-frequency techniques to extract features prior to feeding them into neural networks for recognition, which increases processing time and poses challenges for hardware implementation. Additionally, these methods primarily emphasize performance metrics without considering training time and real-time hardware deployment.

To address the above limitations, this paper proposes a novel automatic signal recognition approach suitable for hardware implementation. This paper is structured as follows: the data acquisition model is presented in Section 2, the theoretical background of the proposed method is described in Section 3, and the simulation and experimental results are provided in Section 4.

2 Received Signal Model

In normal PSS operation, the received signal contains both target echoes and interference [12]. The received signal is defined by (1).

$$s_r(t) = s(t) + n(t) \tag{1}$$

where $s_r(t)$ is the received signal, $s(t)$ is the echo signal from the source and $n(t)$ is the White Gaussian noise. The echo signal is written by (2):

$$s(t) = A\mathrm{e}^{\mathrm{j}(2\pi f_\mathrm{c} t + \phi(t))} \tag{2}$$

where A is the amplitude, f_c is the carrier frequency and $\phi(t)$ is the phase function, which is employed to characterize the intra-pulse modulation.

Intra-pulse modulated radar signals include two main categories: frequency and phase. In this paper, we investigate seven types of intra-pulse modulation signals, including a simple radar pulse, LFM (Linear Frequency Modulation), Costas and polyphase codes (Barker, Frank, P, and Zadoff-Chu). An example of an LFM signal and its amplitude spectrum are shown in Fig. 1.

2.1 Radar Pulse

The first waveform used in radar systems is unmodulated pulse (radar pulse), in which the amplitude, frequency and phase remain constant. The radar pulse is described by (3).

$$s(t)=\begin{cases} A\exp \mathrm{j}\left[2\pi\left(f_{\mathrm{c}}t+\varphi\right)\right] & t\in\left[iT_{\mathrm{op}},\ iT_{\mathrm{op}}+t_i\right] \\ 0 & t\in\left[iT_{\mathrm{op}}+t_i,\ iT_{\mathrm{op}}+t_i+T_M\right] \end{cases} \tag{3}$$

where A is the amplitude, f_{c} is the carrier frequency, T_{op} is the pulse repetition interval (PRI), τ is the pulse width, T_{M} is the pulse off-time, φ is the phase, and i the pulse index.

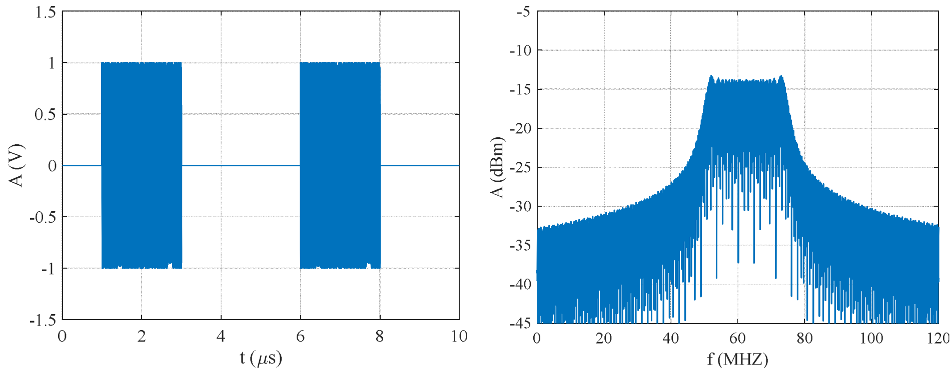

a) b)

Fig. 1 Echo transmitted signal: a) time domain; b) frequency domain

2.2 Linear Frequency Modulation Radar Signal

LFM signal, also known as chirp signal, is characterized by carrier frequency that varies linearly over the pulse width. The LFM signal is typically expressed by (4).

$$s(t)=\begin{cases} A\exp \mathrm{j}\left[2\pi\left(f_{\mathrm{c}}t+\dfrac{kt^2}{2}\right)\right] & t\in\left[iT_{\mathrm{op}},\ iT_{\mathrm{op}}+t_i\right] \\ 0 & t\in\left[iT_{\mathrm{op}}+t_i,\ iT_{\mathrm{op}}+t_i+T_{\mathrm{M}}\right] \end{cases} \tag{4}$$

where $k = BW/t_i$ is the chirp rate and BW is the frequency bandwidth.

2.3 Costas Frequency Coding

Costas frequency coding is widely used in modern radar systems. It maintains constant amplitude and phase while the carrier frequency changes over time according to a Costas code sequence. The general form of Costas signals is given by (5).

$$s(t)=\begin{cases} A\exp \mathrm{j}\left[2\pi\left(f_{\mathrm{c}_n}t+\varphi\right)\right] & t\in\left[iT_{\mathrm{op}},\ iT_{\mathrm{op}}+t_i\right] \\ 0 & t\in\left[iT_{\mathrm{op}}+t_i,\ iT_{\mathrm{op}}+t_i+T_M\right] \end{cases} \tag{5}$$

where f_{c_n} is the carrier frequency of n-th subpulse in the Costas sequence, and typical Costas codes are listed in Tab. 1.

Tab. 1 Common Costas codes

Code length	Code form
Costas 3	1 3 2
Costas 4	1 2 4 3
Costas 5	2 1 5 3 4
Costas 6	1 3 2 6 4 5
Costas 8	2 6 3 8 7 5 1 4
Costas 9	1 3 2 7 4 9 8 6 5

2.4 Binary Phase Shift Keying

In practical radar systems, especially airborne radar, BPSK signals are widely used. These signals have constant amplitude and carrier frequency, while only the phase changes. The general BPSK signal is given by (6).

$$s(t)=\begin{cases} A\exp \mathrm{j}\left[2\pi\left(f_{\mathrm{c}}t+\Delta\psi_k\right)\right] & t\in\left[iT_{op},\ iT_{op}+t_i\right] \\ 0 & t\in\left[iT_{op}+t_i,\ iT_{op}+t_i+T_M\right] \end{cases} \tag{6}$$

where $\Delta\psi_{\mathrm{k}}$ is the phase of each subpulse and 0° for symbol +1 and 180° for symbol −1. Common BPSK signals include Barker codes, as listed in Tab. 2.

Tab. 2 Common Barker codes

Code length	Code forms
Barker 5	+1 +1 +1 −1 +1
Barker 7	+1 +1 +1 −1 −1 +1 −1
Barker 11	+1 +1 +1 −1 −1 −1 +1 −1 −1 +1 −1
Barker 13	+1 +1 +1 +1 +1 −1 −1 +1 +1 −1 +1 −1 +1

2.5 Polyphase Coded Radar Signals

Modern radar systems often employ polyphase coded signals. These signals have constant carrier frequency and amplitude, while the phase varies from one subpulse to another. The general form of the polyphase coded signal is given (7).

$$s(t)=\begin{cases} A\exp \mathrm{j}\left[2\pi\left(f_{\mathrm{c}}t+\varphi_j\right)\right] & t\in\left[iT_{\mathrm{op}},\ iT_{\mathrm{op}}+t_i\right] \\ 0 & t\in\left[iT_{\mathrm{op}}+t_i,\ iT_{\mathrm{op}}+t_i+T_{\mathrm{M}}\right] \end{cases} \tag{7}$$

Polyphase coded signals are typically classified into two main groups: Discrete phase codes (P1, P2, Frank) and continuous phase codes (P3, P4). The phase of each subpulse is defined as follows:

- P1 code

$$\varphi_{a,b} = \frac{-\pi}{M}\left[M-(2b-1)\right]\left[(b-1)M+(a-1)\right] \tag{8}$$

where M is the number of subpulses, a, b are integers and $a,b=1,2,\cdots,M$ are the row and column indices.

- P2 code

$$\varphi_{a,b} = \frac{2\pi}{M}\left(\frac{M+1}{2}-b\right)\left(\frac{M+1}{2}-a\right) \tag{9}$$

where M is the even number.

- Frank code

$$\varphi_{a,b} = \frac{2\pi}{M}(a-1)(b-1) \tag{10}$$

- P3 code

$$\varphi_{a} = \frac{2\pi(a-1)^2}{L} \tag{11}$$

where L is the code length and $a=1,2,\cdots,L$.

3 Proposed Method

The block diagram of the proposed method is shown in Fig. 2. The proposed method consists of three stages:

- estimating pulse width and period of the received signal,
- estimating the instantaneous phase and frequency of received signal,
- recognizing the signal's modulation type using a 1-D deep learning network.

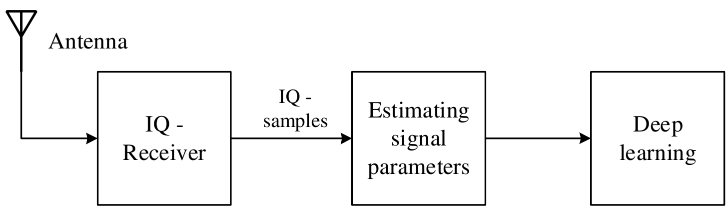

Fig. 2 Block diagram of the proposed method for recognizing intra-pulse modulated radar signals

The first two stages rely on processing the in-phase (I) and quadrature (Q) components of the signal. Therefore, a brief overview of the I/Q data acquisition process is presented first. In recent years, with advancements in science and technology, I/Q receivers, typically referred to as software defined radio (SDR) systems, have become widely adopted. Common examples include HackRF, ANTSDR, and USRP X310. The block diagram of these receivers is shown in Fig. 3.

The SDRs operate based on the following principles: signals of interest captured by the antenna are initially amplified by a low-noise amplifier (LNA). After that, these signals pass through a mixer stage, converting them to baseband signals (zero IF) represented by two quadrature channels (I/Q). Following mixing, the signals undergo filtering to eliminate noise and unwanted components. The bandwidth of filters is in the range of 2 to 120 MHz, depending on the SDR (2 MHz for RTL-SDR, 20 MHz for HackRF, ANTSDR, and 120 MHz for USRP X310). The filtered signals are then digitized via two ADCs (Analog-to-Digital Converter) with resolutions typically of 8 or 12 bits. Finally, the I/Q samples are transferred to computer or FPGA (Field-Programmable Gate Array) via Ethernet or USB (Universal Serial Bus) for digital signal processing [13]. The I/Q data generated by this hardware serves as the input for our feature extraction process, detailed below. The detailed procedures for identifying signal parameters (pulse width and period) and modulation type utilizing these I/Q channels are presented in the next subsection.

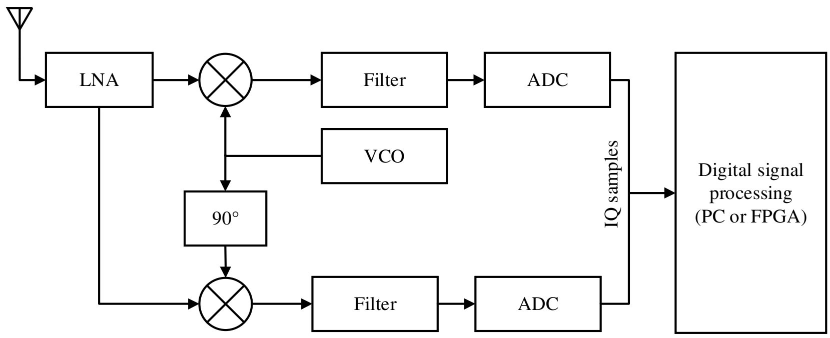

Fig. 3 Block diagram of I/Q receivers

3.1 Signal Parameter Estimation

In digital signal processing [14, 15], using the acquired I/Q signal, the amplitude, instantaneous phase and frequency of the received signals are calculated by (12).

$$\begin{cases} A = \sqrt{I^2 + Q^2} \\ \phi(t) = \arctan \dfrac{Q}{I} \\ f(t) = \dfrac{\mathrm{d}\phi(t)}{\mathrm{d}t} \end{cases} \tag{12}$$

where A is the amplitude, $\phi(t)$ is the instantaneous phase and $f(t)$ is the instantaneous frequency of the received signals. A detailed block diagram of the signal parameter estimation is shown in Fig. 4.

The I/Q signal from the I/Q receiver (the SDR system) is divided into two parallel processing branches. The first branch extracts time-domain parameters by estimating the envelope, removing amplitude variations, and detecting edges to determine pulse width and PRI. The I/Q signal passes through an amplitude extraction block to obtain the envelope by Eq. (12), followed by a pulse normalization stage to generate a clean square-wave representation of the pulse. This normalized pulse is then processed by the edge detection module, where the detected edges serve as the start and end markers for controlling the I/Q data capture in the second branch. These edges are simultaneously used by the pulse width measurement module to determine the pulse width of the incoming radar signal.

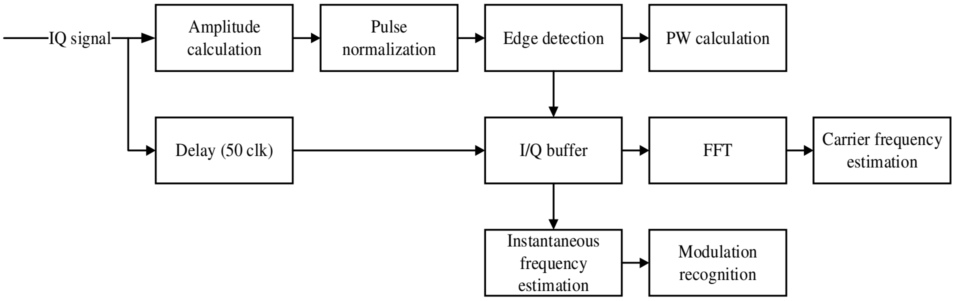

Fig. 4 Block diagram of the signal parameter estimation

In the second branch, the I/Q signal is delayed by 50 clock cycles, ensuring that the buffered I/Q samples correspond exactly to the pulse interval identified in the first branch. After the I/Q buffer stores the pulse segment, the data is split into two processing paths: one path is fed into the FFT block for carrier-frequency estimation, while the other is sent to the instantaneous-frequency estimation module by equation (12). The output of the latter is then forwarded to the modulation-classification unit. All processing stages are implemented on an FPGA operating at a minimum clock frequency of 50 MHz.

3.2 Modulation Recognition

To identify the modulation signals described above, this paper employs a deep learning network whose input consists of the normalized IFE from Section 3.1. The architecture of the deep neural network is illustrated in Fig. 5. The network processes $1 \times 15\,000$ one-dimensional normalized envelopes of instantaneous frequency as input.

- Block 1 consists of a convolutional layer with 32 filters (kernel size 1×5) with same padding, followed by Batch Normalization, a ReLU (Rectified Linear Unit) activation function, and a max pooling layer.
- Block 2 repeats this with 64 filters (1×5), followed by BatchNorm, ReLU, and max pooling.
- Block 3 uses 32 smaller filters (kernel size 1×3) with BatchNorm and ReLU but no pooling, preserving spatial resolution.
- The resulting feature maps are then flattened and fed into a fully connected layer that outputs a 6-dimensional logit vector. A SoftMax activation turns these logits into probabilities over the six signal classes.

4 Simulation Results

In this paper, the performance of the proposed method was evaluated using signals simulated in a MATLAB environment on personal computer (ASUS Vivobook, 16 GB RAM, 2.3 GHz). The intra-pulse modulated radar signals include radar pulse, LFM, Barker, Costas, Frank and P-code with SNR in the range of $[-15, 10]$ dB and $\tau \in [0.1, 2]\,[\mu s]$. The specific parameters for constructing the signal database are detailed in Tab. 3. The simulation includes two steps. The first step is analysing the processing time of all mentioned extracting feature methods, such as: FFT, STFT, WVD and I/Q analysis. The second step is evaluating the AI process.

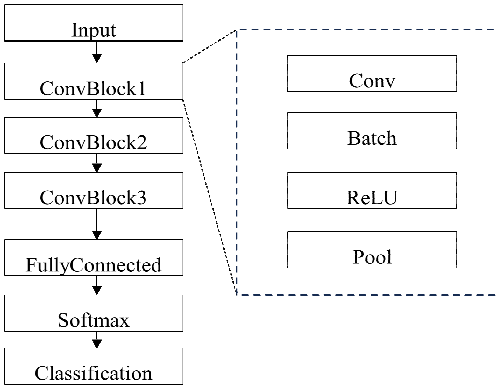

Fig. 5 Structure of the deep learning network for recognizing radar signals

Tab. 3 Signal parameters for constructing the database

Radar signals	Parameters	Value
LFM	BW [MHz]	50 to 100
Costas	Code length	3, 4, 5, 6, 7
	Δf [MHz]	5 to 20
Barker	Code length	7, 11, 13
Frank, P1	Code length	9, 16, 25

Note: All signals are sampled at 1 GHz.

4.1 Processing Time Analysis

Fig. 6 shows the analysis results of the received signals at $SNR = -6$ dB with different methods. Figs 6a and 6b show that the FFT and STFT (Short-Time Fourier Transform) cannot extract the features of radar signals in high noise environments, while the WVD (Wigner-Ville Distribution) and the proposed method are more robust (Figs 6c and 6d). Our proposed method focuses on extracting the instantaneous frequency envelope (IFE). The IFE (the clear red line in Fig. 6d) demonstrates that by measuring rising and falling edges and their slopes, and the signal parameters can be determined. Specifically, the pulse width, repetition period, and frequency deviation are calculated by (13).

From these results, the received signal can be identified as LFM. Its parameters are $\tau = 1.94$ µs, $PRI = 5.0$ µs, $BW = 50.6$ MHz .

$$\begin{cases} \tau_1 = t_2 - t_1 = 2.97 - 1.03 = 1.94 \ \mu\text{s} \\ PRI = t_3 - t_1 = 6.03 - 1.03 = 5.0 \ \mu\text{s} \\ \tau_2 = t_4 - t_3 = 7.97 - 6.03 = 1.94 \ \mu\text{s} \\ BW_1 = f_2 - f_1 = 166.5 - 115.3 = 51.2 \ \text{MHz} \\ BW_2 = f_4 - f_3 = 167.2 - 117.2 = 50.0 \ \text{MHz} \end{cases} \tag{13}$$

The processing times for 500 samples per modulation type, as summarized in Tab. 4 reveal that the WVD method requires the most computational effort ($\bar{t} = 520.03$ s), followed by STFT ($\bar{t} = 2.60$ s), our proposed method ($\bar{t} = 0.72$ s), and FFT ($\bar{t} = 0.48$ s), which is the fastest among them. However, FFT exhibits limitations in accurately extracting features from signals with low probability of intercept (LPI). Based on these findings, we selected the proposed method for feature extraction prior to classification. Due to the wide range of the PSS, received signals often exhibit varying power levels. To mitigate the impacts of these variations, the IFE is normalized prior to the training process.

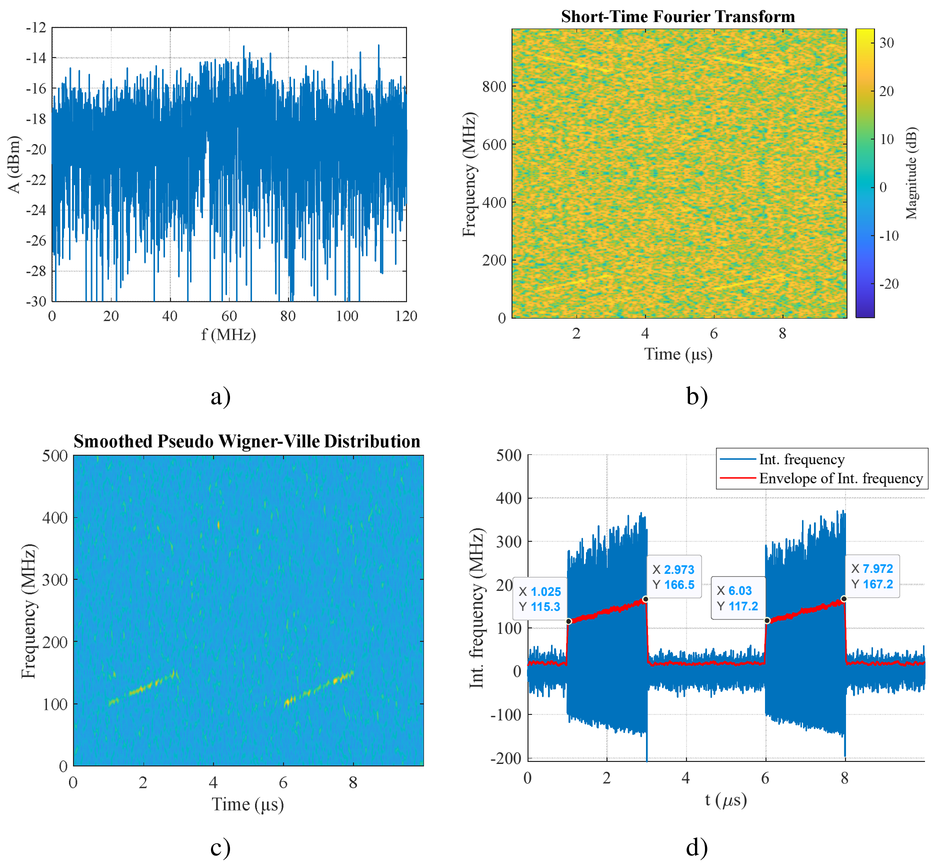

Fig. 6 Analysis results of the received signal with different methods: a) FFT; b) STFT; c) WVD; d) proposed

4.2 Recognition Accuracy Analysis

The general parameters for training the deep learning network are summarized in Tab. 5. This section evaluates the performance of the proposed network using three different input data types: The raw I/Q signals, FFT, and our proposed IFE of signals. While other feature extraction techniques like the STFT and WVD were analysed, they were excluded as inputs for the deep learning network for two main reasons. First, as shown in Tab. 4, their processing times are notably higher, making them impractical for the real-time hardware implementation. Second, these methods generate two-dimensional (2D) time-frequency representations, while the network here is specifically designed with a 1D architecture to efficiently process 1D signals like the proposed IFE. To train the network, the database was partitioned into three parts. The first part (80 %) is for training, second part (10 %) for testing and the last one (10 %) for validation.

Tab. 4 Average processing time for 500 *samples/modulation*

Signals	**Processing time [s]**			
	FFT	STFT	WVD	Proposed
Pulse	0.31	1.32	276.16	**0.35**
LFM	0.27	1.25	243.73	**0.36**
Costas 5	0.47	2.62	470.04	**0.63**
Barker 13	0.87	5.06	989.64	**1.60**
Frank 9	0.45	2.69	442.37	**0.71**
P-code	0.49	2.68	590.23	**0.67**
Average time	0.48	2.60	502.03	**0.72**

Tab. 5 General parameters for training deep learning network

Parameters	Value
Learning rate	0.01
Number of epochs	10
Batch size	32
Activation function	ReLU
Optimizer	Adam

The training time and average recognition accuracies of all mentioned methods are listed in Tab. 6. As presented in Tab. 6, the proposed method demonstrates superior performance in both training efficiency and recognition accuracy. Firstly, our approach significantly reduces training time. With 2 000 samples per modulation type, the proposed method required only $t_1 = 2\,079$ s, whereas the FFT took $t_2 = 3234\ \text{s} = 1.5 \cdot t_1$, and I/Q signal was the slowest at $t_3 = 3899\ \text{s} = 1.9 \cdot t_1$.

Secondly, regarding accuracy, the proposed method consistently achieved the highest performance. With a dataset of 2 000 samples, it reached a recognition accuracy (P_{ra}) of $P_{\text{ra}} = 94$ %, surpassing the FFT ($P_{\text{ra}} = 92$ %) and the I/Q signals ($P_{\text{ra}} = 84.78$ %).

Also, simulation results reveal that a minimum of 1 500 samples per modulation type is needed for both FFT and the proposed method to achieve the desired recognition accuracy ($P_{\text{dra}} \geq 90$ %). Increasing the sample size to 2 000 produces only slight gains (1–3 %), while significantly increasing the required training time. With a small number of samples ($N = 500$, 1 000), none of the methods achieve $P_{\text{dra}} \geq 90$ %.

Tab. 6 Training time and average recognition accuracy of the classification system with different preprocessing methods

Samples/ modulation	Training time [s]			Recognition accuracy [%]		
	I/Q signal	FFT	Proposed	I/Q signal	FFT	Proposed
500	439	342	**240**	67.50	67.50	**70.00**
1 000	1 870	1 118	**852**	72.67	80.33	**85.33**
1 500	3 546	2 929	**1 577**	81.00	90.75	**91.35**
2 000	3 899	3 234	**2 079**	84.78	92.00	**94.00**

Fig. 7 illustrates the recognition accuracy of the proposed network for each intra-pulse modulation signal type. The results indicate that the network performed well on LFM signals (100 %). To achieve the required performance of $P_{dra} \geq 90$ %, $SNR = -12$ dB, $SNR = -10$ dB, and $SNR = -5$ dB are needed for the P1 signal, Costas, and the Frank signal, respectively. However, for the Pulse and Barker signals, the network architecture only achieved a performance of $P_{ra} \leq 85$ %. The authors attribute this limitation to the high similarity of their extracted features, combined with a relatively shallow and unoptimized network architecture. Future work will focus on optimizing the deep learning network architecture to minimize the training time and enhance signal recognition efficiency, especially for these challenging signals.

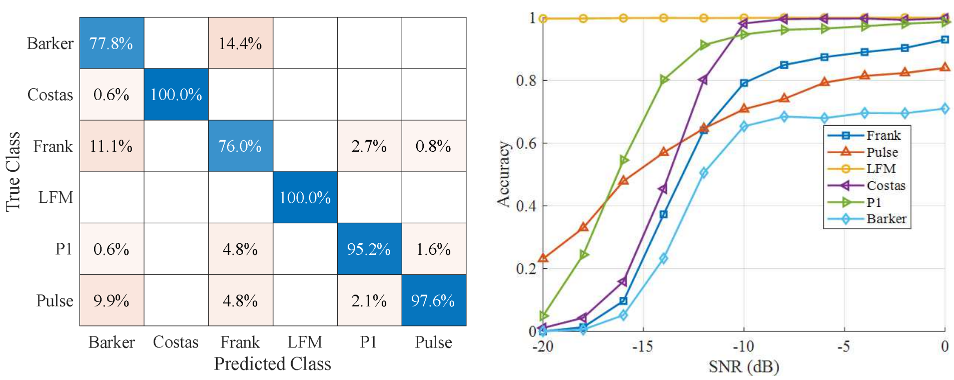

a) b)

Fig. 7 Simulation results: a) confusion matrix; b) accuracy vs SNR

5 Conclusion

The paper introduced a novel two-part algorithm for the recognition of intra-pulse modulation signals. The first part utilizes a digital I/Q receiver for feature extraction and signal parameter estimation. The second part uses a deep learning network for classification based on the extracted features.

The simulation results demonstrate that our feature extraction approach is significantly faster (t = 0.72 s for 500 samples) than conventional methods such as STFT (t = 2.60 s and WVD (t = 502 s). More importantly, when integrated with the deep learning network, the proposed algorithm achieves a high average recognition accuracy (94 %), while requiring substantially less training time compared to models using raw I/Q or FFT data as input. Furthermore, the proposed network results in the highest accuracy for the LFM signal (100 %), followed by P1, Costas, and Frank signals. The required SNRs for $P_{\mathrm{dra}} \geq 90$ % are −12 dB (P1), −10 dB (Costas) and −5 dB for Frank signals. However, the network only reaches a maximum performance of 85 % for Pulse and Barker signals, a limitation we attribute to feature similarity and a sub-optimal network architecture.

In future work, we will focus on optimizing the network architecture to improve recognition for all signal types. Subsequently, the algorithm will be evaluated with real-world signals acquired from a Software-Defined Radio (SDR).

Acknowledgement

This work was supported by a research project: 25.01.34 of Le Quy Don Technical University.

References

[1] WILEY, R.G. *ELINT: The Interception and Analysis of Radar Signals*. London: Artech House, 2006. ISBN 1-58053-926-2.

[2] PHILIP, P. *Detecting and Classifying Low Probability of Intercept Radar*. 2nd ed. London: Artech House, 2008. ISBN 1-59693-235-X.

[3] DAVID, L.A. *Introduction to Electronic Warfare Modelling and Simulation.* London: Artech House, 2003. ISBN 978-1-58053-495-6.

[4] HUBÁČEK, P. and J. VESELÝ. *Základy teorie pasivních systémů IV (Fundamentals of Passive Systems Theory IV)* (in Czech). Brno: University of Defence, 2010. ISBN 80-7231-758-X.

[5] GIRON-SIERRA, J.M. *Digital Signal Processing with Matlab Examples.* Singpore: Springer, 2017. ISBN 978-981-10-2533-4.

[6] HUBÁČEK, P., E. HOŠKO and J. VESELÝ. *Základy teorie pasivních systémů I* (*Fundamentals of Passive Systems Theory I*) (in Czech). Brno: University of Defence, 2007. ISBN 978-80-7231-476-8.

[7] HUBÁČEK, P. and E. HOŠKO. *Základy teorie pasivních systémů II (Fundamentals of Passive Systems Theory II)* (in Czech). Brno: University of Defence, 2008. ISBN 80-7231-614-1.

[8] ZHIYU, Q., H. CHENFAN, H. CHANGBO and W. WENYANG. Radar Signal Intra-Pulse Modulation Recognition Based on Convolutional Neural Network and Deep Q-Learning Network. *IEEE Access*, 2020, **8**, pp. 49125-49136. DOI 10.1109/ACCESS.2020.2980363.

[9] CAI, J., F. GAN, X. CAO, W. LIU and P. LI. Radar Intra–Pulse Signal Modulation Classification with Contrastive Learning. *Remote Sensing*, 2022, **14**(22), 5728. DOI 10.3390/rs14225728.

[10] ZHANG, X., J. ZHANG, T. LUO, T. HUANG, T. TANG and Z. CHEN. Radar Signal Intra-Pulse Modulation Recognition Based on a Denoising-Guided Disentangled Network. *Remote Sensing*, 2022, **14**(5), 1252. DOI 10.3390/rs14051252.

[11] CAI. J., Y. GUO and X. CAO. Automatic Radar Intra-Pulse Signal Modulation Classification Using the Supervised Contrastive Learning. *Remote Sensing*, 2024, **16**(18), 3542. DOI 10.3390/rs16183542.

[12] NADAV, L. and M. ELI. *Radar Signals.* Hoboken: Wiley, 2004. ISBN 0-471-47378-2.

[13] CLARK, P. and D. CLARK. *Introduction to Software Defined Radio*. 2nd ed. Scotts Valley: CreateSpace, 2016. ISBN 1-5368-1476-8.

[14] GOPI, E.S. *Algorithm Collections for Digital Signal Processing Applications Using MATLAB.* Dordrecht: Springer, 2007. ISBN 1-4020-6409-8.

[15] VAN MINH, D., N. THI PHUONG and P. NHAT GIANG. SDR Implemented Algorithms for Real-time Intra-Pulse Modulated Radar Signal Analysis. In*: 2025 10th IEEE International Conference on Integrated Circuits, Design, and Verification (ICDV).* Ho Chi Minh City: IEEE, 2025. DOI 10.1109/ICDV66179.2025.11135420.